A Practical, Hybrid Model for Predicting the Trajectories of Near-Surface Ocean Drifters

NATHAN PALDOR* AND YONA DVORKIN

Institute of Earth Sciences, The Hebrew University of Jerusalem, Jerusalem, Israel

ARTHUR J. MARIANO, TAMAY ÖZGÖKMEN, AND EDWARD H. RYAN

Rosenstiel School of Marine and Atmospheric Sciences, University of Miami, Miami, Florida

(Manuscript received 7 February 2003, in final form 13 February 2004)

ABSTRACT

A hybrid Lagrangian–Eulerian model for calculating the trajectories of near-surface drifters in the ocean is developed in this study. The model employs climatological, near-surface currents computed from a spline fit of all available drifter velocities observed in the Pacific Ocean between 1988 and 1996. It also incorporates contemporaneous wind fields calculated by either the U.S. Navy [the Navy Operational Global Atmospheric Prediction System (NOGAPS)] or the European Centre for Medium-Range Weather Forecasts (ECMWF). The model was applied to 30 drifters launched in the tropical Pacific Ocean in three clusters during 1990, 1993, and 1994. For 10-day-long trajectories the forecasts computed by the hybrid model are up to 164% closer to the observed trajectories compared to the trajectories obtained by advecting the drifters with the climatological currents only. The best-fitting trajectories are computed with ECMWF fields that have a temporal resolution of 6 h. The average improvement over all 30 drifters of the hybrid model trajectories relative to advection by the climatological currents is 21%, but in the open-ocean clusters (1990 and 1993) the improvement is 42% with ECMWF winds (34% with NOGAPS winds). This difference between the open-ocean and coastal clusters is due to the fact that the model does not presently include the effect of horizontal boundaries (coastlines). For zero initial velocities the trajectories generated by the hybrid model are significantly more accurate than advection by the mean currents on time scales of 5–15 days. For 3-day-long trajectories significant improvement is achieved if the drifter's initial velocity is known, in which case the model-generated trajectories are about 2 times closer to observations than persistence. The model's success in providing more accurate trajectories indicates that drifters' motion can deviate significantly from the climatological current and that the instantaneous winds are more relevant to their trajectories than the mean surface currents. It also demonstrates the importance of an accurate initial velocity, especially for short trajectories on the order of 1–3 days. A possible interpretation of these results is that winds affect drifter motion more than the water velocity since drifters do not obey continuity.

1. Introduction

In this work we develop a method for reconstructing observed trajectories of near-surface drifters in the Pacific Ocean by incorporating climatological currents with real-time winds. Accurate prediction of (near) surface particle trajectories, in the ocean, is of paramount importance for a number of operational activities, such as search and rescue and monitoring the spread of pollutants. Prediction of particle trajectories is extremely difficult because the uncertainties in our knowledge of the ocean's flow field and its forcing functions are quickly amplified by the chaotic nature of nonlinear advection (Aref 1984, 1990). This inherent limitation of the predictability of ocean particle trajectories facilitates optimal use of data. Available data that can be used for trajectory prediction consist primarily of either historical sea surface velocity measurements from ship drift (Mariano et al. 1995) and buoys (Niiler 2001), sea surface height (Lagerloef et al. 1999) and mixed-depth climatologies (Rao et al. 1989), or (quasi) real-time data such as wind, drifting buoys, and sea surface height anomalies from satellites (e.g., TOPEX/Poseidon). In addition, numerical models can be used to simulate particle trajectories and/or provide Eulerian velocity estimates on a regular space–time grid for input into a Lagrangian-based prediction model. The numerical models' complexity ranges from simple (in the Eulerian sense) analytical models for the flow field that only contain a few adjustable physical parameters (e.g., Bow-

* Additional affiliation: MPO/Rosenstiel School of Marine and Atmospheric Sciences, University of Miami, Miami, Florida.

Corresponding author address: Dr. Tamay Özgökmen, University of Miami/RSMAS, MPO Division, 4600 Rickenbacker Causeway, Miami, FL 33149-1098.
E-mail: tozgokmen@rsmas.miami.edu

er 1991; Dutkiewics and Paldor 1994) to high-resolution ocean circulation models that have more parameters and require initial and forcing fields (Garraffo et al. 2001a,b; Garfield et al. 2001; McClean et al. 2002). The optimization of available data for Lagrangian prediction is a difficult problem because (a) the turbulent flow field is highly nonlinear in many oceanic regimes; (b) there exists a wide range of available data with different (i) space–time resolution that is usually sparse, (ii) error characteristics, and (iii) measurement type, for example, Eulerian, isobaric, mixed layer, and (quasi) Lagrangian; and (c) there is also a hierarchy of dynamical and statistical models. Exhaustive testing with in situ ocean data and extensive Monte Carlo simulations are necessary for evaluating different prediction models and different input data because the optimization is highly nonlinear and practical requirements dictate predictions for short time scales of a week or less. On these time scales, Lagrangian motion is sensitive to initial conditions (Davis 1982; Flierl 1981) and asymptotic theories for turbulent dispersion do not apply.

Models of the oceanic velocity field traditionally assume it can be decomposed into a large-scale mean field, a turbulent field consisting of both correlated velocity fluctuations and random fluctuations, and a component forced by winds, pressure gradients, and rotation. The simplest such models assume that the velocity field $\mathbf{u}$ is given by

$$\mathbf{u} = \mathbf{U} + \mathbf{u}', \tag{1.1}$$

where $\mathbf{U}$ is the large-scale mean velocity, usually derived by either forming a climatological average of all available velocity data, fitting a few basis functions to local subsets of the data, using the output of a numerical model, or based on a simple analytic expression for the flow field. The turbulent velocity components, $\mathbf{u}'$, have been modeled as Brownian diffusion, as a Markov or autoregressive (AR) model of order one, and, recently, as higher-order AR(2) and AR(3) models (Griffa 1996; Pasquero et al. 2001; Berloff and McWilliams 2002). As the model order increases, so do the number of parameters that need to be estimated for each velocity component. In particular, an AR(1) model for a discrete time process sampled at equal time increments Δt is of the form

$$\mathbf{u}'(t) = a\mathbf{u}'(t - \Delta t) + \varepsilon, \tag{1.2}$$

where ε is a (two dimensional) Gaussian-distributed process with zero-mean and prescribed variance and $a = (1 - \Delta t/T)$, where T is the integral time scale calculated by integrating the Lagrangian velocity covariance function, $\mathbf{R}(\tau)$, over all positive values of τ, that is,

$$T = \int_0^\infty \mathbf{R}(\tau)\, d\tau. \tag{1.3}$$

Model (1.2) is the random flight model and was introduced into meteorology by Thomson (1986, 1987). It has been the model of choice in a few recent oceanographic dispersion analyses (Bauer et al. 1998) and Lagrangian predictability studies (Özgökmen et al. 2000, 2001; Castellari et al. 2001). This model is a good approximation if the observed form of $\mathbf{R}(\tau)$ decays exponentially. However, if $\mathbf{R}(\tau)$ contains significant negative sidelobes (indicating wave processes), then an AR(2) model should be used instead of the AR(1) model (1.2). The relevant parameters for an AR model for $\mathbf{u}'$ in Eq. (1.1) in this region were estimated by Bauer et al. (1998, 2002) using a larger set of drifters.

An alternate, dynamical approach for calculating horizontal velocities is a forced particle model on a rotating sphere, proposed by Dvorkin et al. (2001) and Paldor et al. (2001) for reconstructing the trajectories of constant-level balloons in the atmosphere. This model has successfully reconstructed balloon trajectories in both the tropical stratosphere and extratropical troposphere by assuming that the advection of a particle consists of the (weighted) sum of the airflow given by the European Centre for Medium-Range Weather Forecasts (ECMWF) standard fields and a ''correctional'' velocity. The latter was determined from a Lagrangian dynamical model that included pressure gradient forcing (determined from the gradient of Montgomery streamfunction), rotation (i.e., Coriolis), and Rayleigh friction.

In the present study, we adopt a similar approach to that of Eq. (1.1) for surface drifters in the Pacific Ocean, but instead of modeling $\mathbf{u}'$ in Eq. (1.1) (i.e., the turbulent velocity) we model $\mathbf{U}$ using a Lagrangian dynamical model that incorporates instantaneous winds and climatological surface currents into the drifter-forced motion.

A key element in our hybrid Lagrangian model is the incorporation of the wind stress in the motion of near-surface drifters. In state-of-the-art ocean circulation models, this element requires a complex turbulence closure scheme, but in the simplest model, one assumes a uniform slab of water over which the observed wind stress is uniformly distributed. The only physical parameter in this slab model is the Ekman (or approximately the mixed layer) depth.

A similar approach was applied by Lagerloef et al. (1999), who employed a steady-state model where the velocities of a surface slab of mean depth h are the solution of the system:

$$-fhv = -gh(\partial\eta/\partial x) + \tau^x/\rho - ru_e, \tag{1.4a}$$

$$fhu = -gh(\partial\eta/\partial y) + \tau^y/\rho - rv_e, \tag{1.4b}$$

where f is the Coriolis parameter, η is the sea surface height, (τ^x, τ^y) are the horizontal wind stress components, r is the Rayleigh friction coefficient, u_e and v_e are Ekman components of the velocity field, and $\rho = 1025$ kg m^{-3} is the water density. The various data required as forcing on the right-hand side include near-surface World Ocean Circulation Experiment (WOCE)/

Tropical Ocean Global Atmosphere (TOGA) drifters in the tropical Pacific at a nominal depth of 15 m; 10-m current velocities from the TOGA Tropical Atmosphere Ocean (TAO) array; Special Sensor Microwave Imager (SSM/I) winds; and sea surface height anomalies from TOPEX/Poseidon. These were used in fitting the model parameters to the observed currents by least squares. The mean mixed layer depth, h, was found by Lagerloef et al. (1999) to be (32 ± 1.2) m, and their Rayleigh friction parameter, r, is $(2.15 \pm 0.3)10^{-4}$ m s^{-1}, that is, a velocity relaxation time, h/r, of order 1.5 days.

In comparison to these estimates, a time-dependent, wind-forced slab model, originally proposed by Pollard and Millard (1970), has successfully reproduced the observed currents in various oceanographic settings (see, e.g., Kundu 1976; Käse and Olbers 1979) with a velocity relaxation time between 2 and 8 days and mixed layer depth of 45–55 m. The velocity relaxation time that emerges from all these slab, mixed layer models is on the order of a few days. As for the Ekman depth, the estimate by Lagerloef et al. (1999) of about 30 m is more relevant to our study since it is derived in the same geographic location.

Both the drifter trajectories generated by the hybrid model and those due to advection by the climatological surface currents are compared to observed drifter trajectories in order to assess the improvement afforded by the model. We selected surface drifter trajectories from the tropical Pacific to quantify the performance of our hybrid model in reconstructing drifter trajectories. This region was chosen for a number of reasons: 1) there are a number of drifters that were launched in tight clusters, so that we can evaluate the model's performance over a number of different realizations in a given area and time; 2) the area is rich in ocean phenomena with equatorial jets and a strong eddy motion; and 3) a number of different analyses that are required for this quantification in the present study were already available to us. Bauer et al. (1998) calculated mean fields, integral time scales, and diffusivities for these drifters. The results of Bauer's study indicate that an AR(1) model for each turbulent Lagrangian horizontal velocity component is a good assumption for our analysis domain.

The remainder of this paper is organized as follows. In section 2 we develop the governing equations of the hybrid model. Section 3 provides the details of the various sources of data used for quantifying the improvement afforded by the hybrid model, and the methods in which these data were employed. Section 4 contains the results of the application of the hybrid model to reconstruct the observed trajectories. We end in section 5 with concluding remarks.

2. The hybrid model

The hybrid model, employed in the present study, is an adaptation of the atmospheric hybrid model for calculating the trajectories of high-altitude, constant-level balloons described in Dvorkin et al. (2001) and Paldor et al. (2001). The underlying concept of the model is that drifters fully obey the same Newton's second law of motion as water columns. However, nearby launched drifters are observed to diverge much faster than the horizontal divergence of water columns in the surface layer (e.g., Fig. 4 of Paduan and Niiler 1993). This fast divergence, as seen by the convergence of seaweed and plastics at the surface, implies that in contrast to water columns drifter trajectories are not constrained by the continuity equation that links the pressure gradient force with the divergence of the horizontal velocity. The correction velocity, $\mathbf{V}_{\rm cor}$, which differentiates between the climatological surface velocity field, $\mathbf{V}_{\rm clim}$, and the drifter's velocity, $\mathbf{V}_{\rm dr}$, is calculated from Newton's second law of motion by taking into account the best available estimates of all forces known to act on the drifter. The correction velocity is then linearly combined with the climatological velocity field to yield the model drifter velocity according to

$$\mathbf{V}_{\rm dr} = \alpha\mathbf{V}_{\rm cor} + (1 - \alpha)\mathbf{V}_{\rm clim}, \tag{2.1}$$

where α measures the fraction of drifter velocity contributed by the correction velocity, that is, its deviation from the climatological velocity at its location.

We use a slab model for calculating the dimensional (denoted by an asterisk) correction velocity $\mathbf{V}^*_{\rm cor} = (u^*_{\rm cor}, v^*_{\rm cor})$ of a drogued drifter of vertical span H (i.e., the surface buoy and the drogue represent the velocity over an Ekman depth H). The vertically averaged (between $z = -H$ and $z = 0$) momentum equations on earth (no planar approximation) are (see Gill 1982)

$$du^*_{\rm cor}/dt = v^*_{\rm cor}\sin(\phi)[2\Omega + u^*_{\rm cor}/R\cos(\phi)] + \Gamma^x/H - \gamma^* u^*_{\rm cor} \tag{2.2a}$$

and

$$dv^*_{\rm cor}/dt = -u^*_{\rm cor}\sin(\phi)[2\Omega + u^*_{\rm cor}/R\cos(\phi)] + \Gamma^y/H - \gamma^* v^*_{\rm cor}. \tag{2.2b}$$

In system (2.2), Ω and R are the earth's frequency of rotation and radius, respectively; ϕ is the latitude; $\Gamma^x(\Gamma^y)$ is the wind stress at the ocean's surface in the zonal (meridional) direction divided by the density of water; and γ^* is the Rayleigh friction coefficient. Thus, $1/\gamma^*$ is the velocity relaxation time, that is, the time it takes the velocity to settle back to e^{-1} of its value after the wind ceases to blow.

These equations are nondimensionalized (e.g., Paldor and Killworth 1988) by scaling time and length by $1/(2\Omega)$ and R, respectively. The resulting velocity scale, $2\Omega R$, is 931 m s^{-1}, so nondimensional oceanic velocities are of order 10^{-3}. The nondimensional form of (2.2) is

$$du_{cor}/dt = v_{cor}\sin(\phi)[1 + u_{cor}/\cos(\phi)] + \tau^x/\delta - \gamma u_{cor} \quad (2.3a)$$

and

$$dv_{cor}/dt = -u_{cor}\sin(\phi)[1 + u_{cor}/\cos(\phi)] + \tau^y/\delta - \gamma v_{cor}. \quad (2.3b)$$

Here, all variables are nondimensional, so $\tau^x(\tau^y)$ is $\Gamma^x(\Gamma^y)$ scaled by $(2\Omega R)^2$, and $\delta = H/R$. The parameter δ is not incorporated into the wind stress, $\boldsymbol{\tau}$, since we wish to be able to examine the effect that changes in H have on the dynamics separately from the effect of the wind stress. The time scale of $1/(2\Omega) = 1$ day$/(4\pi) = 6/\pi$ h implies that a dimensional relaxation time, $1/\gamma^*$, of N days corresponds to a nondimensional Rayleigh friction coefficient, γ, of $1/(4\pi N) = 0.08/N$.

Once the correction velocity is calculated based on the wind field and the drifter's location, the drifter is advected to new coordinates according to

$$d\phi/dt = v_{dr} = \alpha v_{cor} + (1 - \alpha)v_{clim}, \quad (2.3c)$$

$$d\lambda/dt = u_{dr}/\cos(\phi) = [\alpha u_{cor} + (1 - \alpha)u_{clim}]/\cos(\phi). \quad (2.3d)$$

In the practical application of model equation (2.3) the time derivatives on the left-hand side are computed at the drifter position, that is, in the Lagrangian formulation. At each integration time step the gridded values of both wind stress, $\boldsymbol{\tau}$, and climatological velocity $\mathbf{V}_{clim}$ are interpolated to the drifter location. The next section provides the details of the data sources for both fields and the way they are interpolated to the drifter location. For each of the observed drifter trajectories, system (2.3) was integrated, starting from the drifter's launch position, in time steps of 0.1 nondimensional time units, about 11 min so that the error of the fifth-order integration scheme does not exceed 10^{-5}. The initial velocity was assumed either zero, simulating real cases in which the initial velocity is not known, or known from the first velocity data point. Given the ever-increasing use of GPS-tracked emergency beacons, initial positions and velocities may be available in practical applications. The effect of known initial velocities is detailed in section 4.

Since the wind stress and climatological fields are given only every 6 or 24 h, temporal interpolation into integration time steps is also required, which was done by bicubic splines (see section 3 for more details on the interpolation scheme). By integrating Eqs. (2.3c) and (2.3d) one gets the new drifter position. This procedure is repeated for $40N\pi$ nondimensional time steps, yielding an N-day-long trajectory $[\lambda(t), \phi(t)]$. The computed trajectory for the prescribed values of α and γ is then compared to the observed trajectory of the particular drifter being simulated. Many trajectories with different (α, γ) values were estimated for each drifter in the clusters listed in Table 1. The average separation between the simulated and observed drifter trajectory, as a function of these parameters, different wind products, and knowledge of initial velocity, is quantified in section 4.

TABLE 1. Summary of number of drifters in the three clusters used here and their launch sites and dates.

Cluster	No. of drifters	Launch site	Launch date
1990	16	5°N, 220°E	18–22 Nov
1993	5	5°S, 270°E	25 Oct
1994	9	20°N, 200°E	5–7 Oct

3. Data and methodology

The data sources used (drifter trajectories, climatological near-surface currents, and wind stress fields), and the way they were incorporated in the hybrid model, are described here.

a. Data sources

1) DRIFTER TRAJECTORIES

Drifter trajectories from the archive of near-surface drifters of the National Oceanic and Atmospheric Administration (NOAA) Atlantic Oceanographic and Meteorological Laboratory (AOML) are used for evaluating different numerically generated trajectories. These ARGOS-tracked drifters are drogued with a 1-m-diameter holey sock centered at 15 m. [More details on the drifters' design, tracking, and data processing are provided in Hansen and Poulain (1996), and online at http://www.aoml.noaa.gov/phod/dac/dacdata.html.] The drifter data used here are the krigged drifter positions with a temporal resolution of 6 h.

The three drifter clusters we used for quantifying the hybrid model's improvement have also been analyzed by Özgökmen et al. (2001). They performed trajectory predictions using a simplified Kalman filter that assimilates significantly correlated, contemporaneous Lagrangian data into the random flight model—Eq. (1.1). The Özgökmen et al. (2001) work provides bounds on the Lagrangian prediction error that can be expected in the present study. The expected error in the present study should be smaller than that given by turbulent dispersion (50–150-km rms spread over 7 days) but larger than the prediction error when contemporaneous data are assimilated (about 15 km for a 7-day prediction).

A summary of the number of drifters in each of the three clusters used here, and the time and location of launch, is given in Table 1. The first N-day segment of each of the drifter trajectories in Table 1 was simulated using the hybrid model described in section 2. In Fig. 1 we provide the geographical location of the launch site of each cluster in the tropical Pacific.

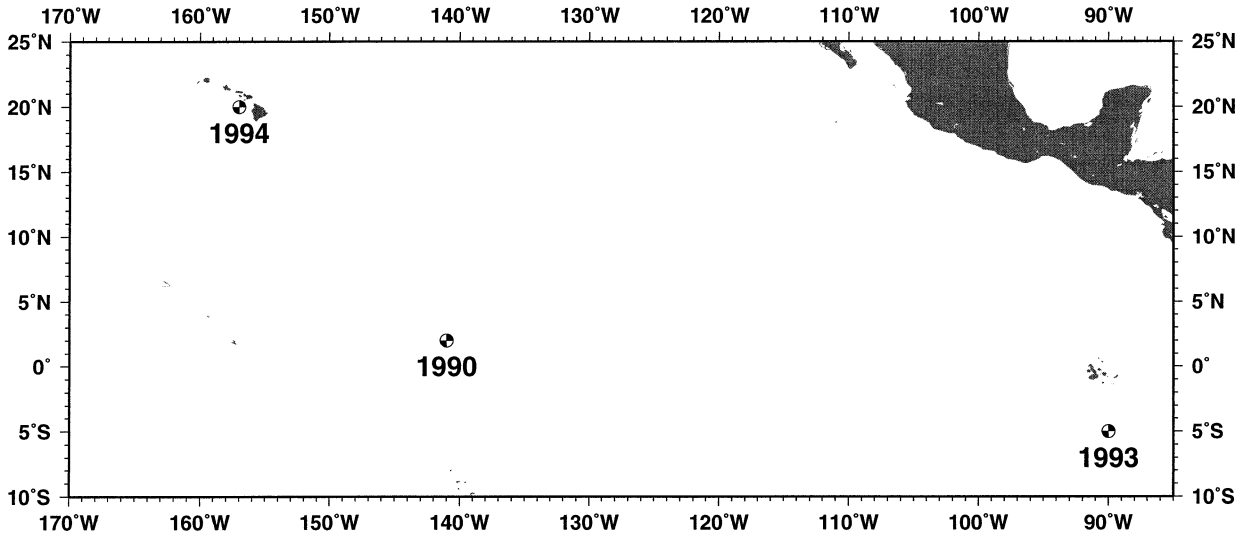

FIG. 1. Study area of the three drifter clusters used in this study (see Table 1 for more details).

2) CLIMATOLOGICAL NEAR-SURFACE CURRENTS

Climatological near-surface ocean currents were constructed from the 1988–96 WOCE drifter dataset by using the interpolation technique developed by Bauer et al. (1998). Briefly, velocity time series along an individual drifter trajectory was calculated from krigged position data using the technique detailed in Hansen and Poulain (1996). Bicubic least squares smoothing splines were then fitted to monthly subsets of each drifter velocity component, $u(\lambda, \phi, t)$ and $v(\lambda, \phi, t)$, to form the large-scale mean velocity field, $u_{\text{clim}}(\lambda, \phi)$ and $v_{\text{clim}}(\lambda, \phi)$, as a function of longitude λ and latitude ϕ with a spatial resolution of 0.1°. Figure 2 shows the climatological, near-surface currents in the areas where the three clusters used in the present study were launched.

3) WIND STRESS FIELDS

For wind stress forcing (Γ^x and Γ^y) we used two fields. The first is the Navy Operational Global Atmospheric Prediction System (NOGAPS) wind stress estimates from 1990 to 1996, produced at a horizontal resolution of 1.25° and a temporal resolution of one field per day. [These data are available from The Florida State University (FSU), Web site: http://www.coaps.fsu.edu/WOCE/SAC/models/nogaps/.] We have also used the ECMWF wind stress for the years 1990 and 1993 to make sure our results are not specific to NOGAPS winds. These fields have a similar spatial resolution of 1.125° but a 4-times-higher temporal resolution of one field every 6 h. However, these wind fields are not as freely available as the NOGAPS fields. Consequently, ECMWF wind fields were not used for the 1994 cluster that is near the coast of Hawaii.

b. Application of the various data in the hybrid model

The wind stress and climatological current were interpolated to the numerically generated drifter location from the gridded values at each integration time step (recall that the integration time step is 11 min = 0.1 nondimensional units). The observed locations from the N-day trajectory of each drifter were interpolated to an equidistant time series of 0.1 nondimensional time intervals to enable a quantification of the distance between observed and calculated trajectories at every time step (see exact formula in the following section). The interpolation scheme that produced the results described in the next section was a bicubic spline with three points on each side in both space and time. An application of a much simpler, linear interpolation scheme resulted in only slightly less accurate trajectories and a somewhat shorter run time.

Most of our results were computed with an Ekman depth of 30 m [i.e., $\delta = (30\text{ m})/R$ in Eqs. (2.3a,b)], in accordance with the mixed layer (Ekman) depth found by Lagerloef et al. (1999), but we have also experimented (see section 4) with other Ekman depths.

4. Results

Each of the calculated trajectories was initiated with its $[\lambda(0), \phi(0)]$ set by the launching site (longitude, latitude) of an observed drifter trajectory (designated by #i), and its initial velocity $[u(0), v(0)]$ was set to zero. Examples of the trajectories that result from known initial velocities are described at the end of this section. The difference between the N-day-long trajectory calculated for given (α, γ) values and the corresponding observed trajectory of drifter #i was quantified by measuring the mean separation between the two trajectories

over the course of N days ($4N\pi$ nondimensional time units), as follows. The instantaneous separation at time $t_j = j \cdot \delta t$ ($\delta t = 0.1, j = 0, \ldots, 40N\pi$) between observed drifter #i and its numerical counterpart is simply the length of the arc (on a unit sphere) that connects their (longitude, latitude) coordinates. Thus, the nondimensional instantaneous separation at time $j \cdot \delta t$ is

$$D_i^j(\alpha, \gamma) = \cos^{-1}[\sin(\phi_1)\sin(\phi_2) + \cos(\phi_1)\cos(\phi_2)\cos(\lambda_2 - \lambda_1)], \quad (4.1)$$

where (λ_1, ϕ_1) and (λ_2, ϕ_2) are the observed and calculated positions of drifter #i at time $j \cdot \delta t$.

The average separation of the two trajectories between $t = 0$ and $t = J \cdot \delta t$ is therefore, simply

$$D_i^J(\alpha, \gamma) = \frac{1}{J}\sum_{j=1}^{J} D_i^j(\alpha, \gamma). \quad (4.2)$$

The mean separation during the entire N-day-long trajectory $D_i(\alpha, \gamma)$ is defined as D_i^J for $J = 40N\pi$ in Eq. (4.2), which is a measure of the mean error of the numerical trajectory generated by the hybrid model with the particular (α, γ) values in simulating observed trajectory #i. The average of the $D_i(\alpha, \gamma)$ values of M trajectories (each designated by subscript i), $D(\alpha, \gamma) = (1/M)\,\Sigma\, D_i(\alpha, \gamma)$, is a more reliable quantitative estimate of how well the hybrid model simulates drifter trajectories for particular (α, γ) values used for predicting all M observed trajectories.

Recall from its definition that $\alpha = 0$ implies advection of the drifter by the climatological surface current only. Accordingly, the improvement factor of the hybrid model with given values of α and γ relative to pure advection by the mean surface currents for all drifters, IF(α, γ), is defined as the ratio between the two D values, that is,

$$\mathrm{IF}(\alpha, \gamma) = D(\alpha = 0)/D(\alpha, \gamma) = \frac{\sum_{i=1}^{M} D_i(\alpha = 0)}{\sum_{i=1}^{M} \mathrm{D}_i(\alpha, \gamma)} \quad (4.3)$$

(improvement is achieved for IF > 1.0), and the improvement factor for a particular drifter #i is

$$\mathrm{IF}_i(\alpha, \gamma) = D_i(\alpha = 0)/D_i(\alpha, \gamma). \quad (4.4)$$

Note that there is no simple relationship between IF(α, γ) and IF$_i(\alpha, \gamma)$ since the former is the ratio between the *sum* of $D_i(\alpha = 0)$ over all i and the *sum* of $D_i(\alpha, \gamma)$, while the latter is the ratio between values of $D_i(\alpha = 0)$ and $D_i(\alpha, \gamma)$, that is, for a *particular* i as prescribed in Eq. (4.4).

From its definition it is clear that higher IF > 1.0 values indicate more significant improvement of the hybrid model for the particular (α, γ) values compared to advection by climatology ($\alpha = 0$).

The IF(α, γ) contours were calculated from a large (including unrealistically long relaxation times) matrix of (α, γ) values spanning the ranges $\alpha = [0.001, 0.002, \ldots, 0.009, 0.01, 0.02, \ldots, 0.99, 1.0]$ and $\gamma = [0, 0.001, 0.002, \ldots, 0.009, 0.01, 0.02, \ldots, 0.99, 1.0]$, as well as for $\alpha = 0$ (when the value of γ does not affect the trajectory). Thus, the total number of runs [i.e., pairs of (α, γ) values] for each of the 30 drifters was 110*109 + 1 = 11 991. This choice of the number of pairs enables both high resolution at small (α, γ) values and a

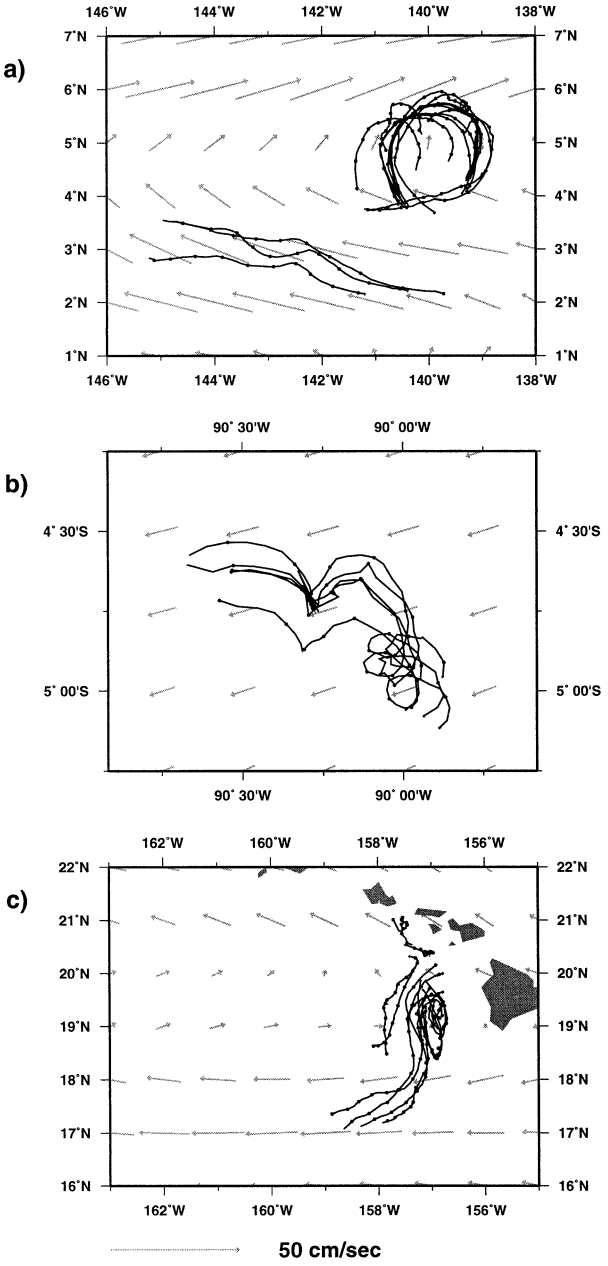

FIG. 2. Drifter trajectories in (a) the 1990 cluster, (b) the 1993 cluster, and (c) the 1994 cluster, and the annual-mean, climatological, near-surface, velocity fields for each study area. Closed circles along the trajectories mark 1-day intervals. Velocity fields are subsampled for clarity of presentation.

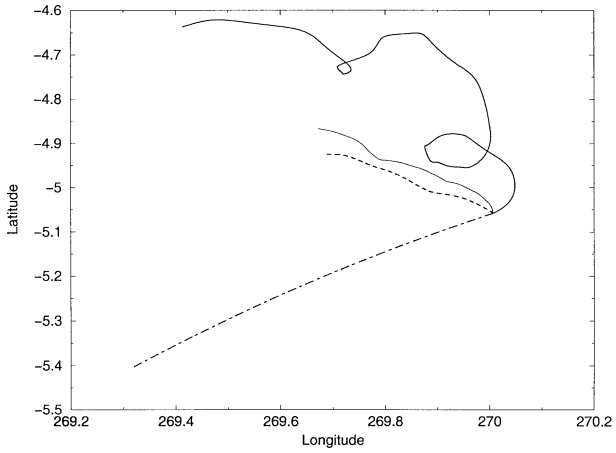

FIG. 3. An example of an observed trajectory (of drifter no. 25 of the 1993 cluster, thick solid curve), the trajectory obtained from advection by the climatological currents (dot–dashed curve), and the trajectory calculated by the hybrid model with the ECMWF winds (thin solid curve; IF = 2.640) and the NOGAPS winds (dashed curve; IF = 2.321).

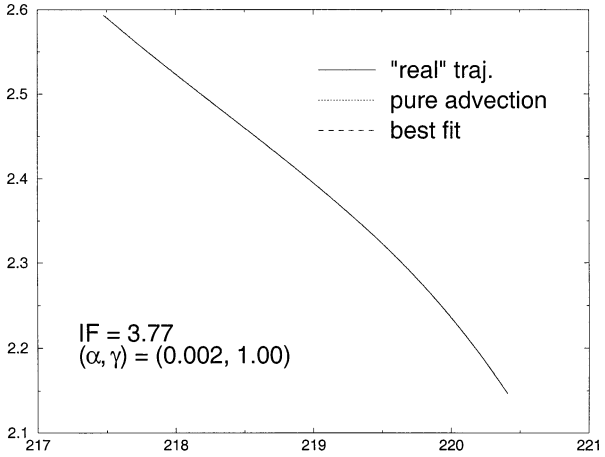

FIG. 4. The hybrid model's result for a ''numerical'' trajectory generated by the climatological currents. The best IF of 3.77 obtains at $\alpha = 0.002$; i.e., an addition of a very small correctional velocity component improves the pure advection drastically when the latter is a good predictor.

sufficiently dense grid for producing the IF contours. Values of γ larger than 1.0 represent fast relaxation times (shorter than $6/\pi \approx 1.9$ h), and they produced small IF values in all cases (see below) since the drifter hardly moves at all from its initial position. Most computations in the next subsections were done for $N = 10$ days, in line with estimates of Özgökmen et al. (2001), but other trajectory lengths were also considered.

a. Best trajectories of the hybrid model

The relevant, 10-day-long trajectories of drifter number 20025 (this is the drifter's ID number at AOML archive) of the 1993 cluster are shown in Fig. 3 for both NOGAPS (dashed curve) and ECMWF (thin solid curve) winds with zero initial correctional velocity. The (α, γ) values that yield the best trajectories are (1.00, 0.08) for ECMWF winds and (1.00, 0.16) for NOGAPS winds, and the $\text{IF}(\alpha, \gamma)_{20025}$ values of these trajectories are 2.640 and 2.321, respectively. Thus, the hybrid model's trajectories are over 164% (132% for NOGAPS) closer to the observed trajectory (thick solid curve) than the trajectory due to pure advection (dot–dashed curve). Note that $\alpha = 1.0$ yields the best trajectory for both wind fields; that is, the climatological, near-surface currents play only a negligible role, if any, in the advection of the drifter.

When the simulated trajectory of this same drifter was initialized with the observed velocity provided by AOML [i.e., by letting $\mathbf{V}_{\text{cor}}(t = 0) = [\mathbf{V}_{\text{obs}} - (1 - \alpha)\mathbf{V}_{\text{clim}}]/\boldsymbol{\alpha}$, where $\mathbf{V}_{\text{obs}}$ is the observed drifter velocity at $t = 0$] the resulting best IF value with ECMWF forcing is 3.424 compared with 2.640 in the case of zero initial velocity described above [i.e., when $\mathbf{V}_{\text{cor}}(t = 0) = 0$ is assumed].

The two IF values of the particular observed trajectory shown in Fig. 3 are the highest of all 30 trajectories (i.e., 11 991*30 = 359 730 IF values) simulated in this study [with $\mathbf{V}_{\text{cor}}(t = 0) = 0$], but other simulated trajectories have IF values close to these best ones. Obviously, there are (α, γ) values that yield $\text{IF}_i(\alpha, \gamma) < 1.0$ for some drifters, so no general conclusion can be reached based on a single trajectory simulation. A wide range of best α values is expected given the high variability of drifter trajectories due to the energetic eddy field that is not captured in the climatology nor by the simple particle model. In order to ascertain that in simple (artificial) cases the hybrid model produces the expected results, we applied the model to an ''observed'' trajectory generated from the climatological currents. One expects the hybrid model to yield a good fit with $\alpha = 0$ and the best fit with $\alpha \cong 0$, both of which are, indeed, the result shown in Fig. 4, where $D(\alpha = 0) = 6.353 \times 10^{-5}$, $D(\alpha = 0.002, \gamma = 1.0) = 1.685 \times 10^{-5}$.

Two important conclusions can be reached from this trivial experiment on the interpretation of the hybrid model results for a single drifter. The first is that a large IF value (i.e., 3.77) obtains even when the best-fitting trajectory is not significantly different from pure advection. This occurs when the latter is close to the observed trajectory so that a slightly improved trajectory yields a tiny denominator in Eq. (4.4) (i.e., ''zero'' divided by ''zero'' can yield a very large value). The second conclusion relates to the proper interpretation of the (α, γ) values that yield the best-fitting trajectory: sufficiently small values of α should be considered as 0.0, and the value of γ should only be interpreted for its order of magnitude. The result shown in Fig. 4 raises the important issue of the robustness of the results to slight changes in the parameter values. This point will be addressed shortly, when averaged IF values for several drifters (belonging to one or more clusters) will be

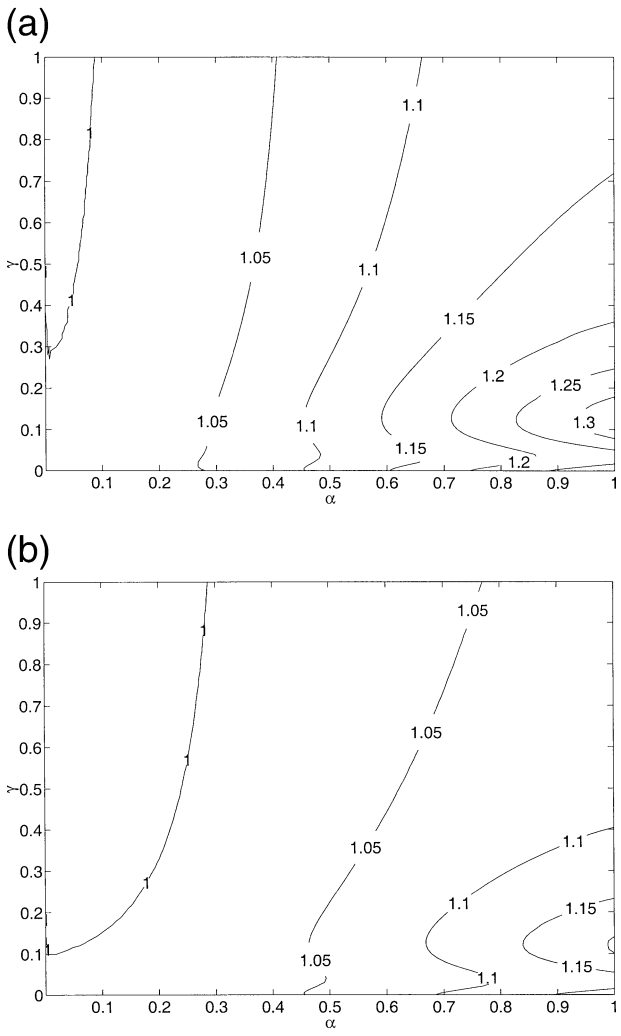

FIG. 5. Contour plot of IF(α, γ) obtained with NOGAPS wind stress for (a) open-ocean 1990 and 1993 clusters and (b) all three clusters. Very few (α, γ) pairs yield IF < 1.0 in the open-ocean clusters shown in (a) where the minimal IF value is 0.999, and with $\alpha > 0.6$ the IF values exceed 1.1 for nearly all γ values. The addition of the Hawaiian 1994 cluster [shown in (b)] lowers all IF values since the boundary conditions associated with the presence of coastlines are currently ignored in the model.

employed to quantify the hybrid model's improvement in various circumstances and for different (α, γ) values.

b. Open-ocean and coastal drifters

Figures 5a and 5b are contour plots of the average IF(α, γ) over the 21 open-ocean trajectories of the 1990 and 1993 clusters and the average IF over 30 trajectories in all three clusters, respectively, for NOGAPS winds. These results, obtained for 10-day-long trajectories, show that in both cases the best IF values occur at $\alpha = 1$ and $\gamma = 0.12$ (relaxation time of 16 h), which demonstrates the following points.

The first point is the weakness of the present hybrid model in handling coastlines, which is clearly evident in the comparison between Fig. 5a and Fig. 5b. The 1994 cluster was launched near the islands of Hawaii (see Fig. 1) that affect the observed drifter trajectories by imposing the no-normal-flow condition. The climatological currents do not flow normal to the coastline. The no-normal-flow boundary condition is not imposed on the correctional velocity [i.e., Eqs. (2.3a) and (2.3b)] in the particle model, and some of the predicted trajectories, with $\alpha \neq 0$, pass over land. For $\alpha > 0$ improvement (over pure advection) using the particle model is not expected near the coasts since the coastal boundary conditions are ignored, and because these wind products do not contain the smaller and faster phenomena near land–sea boundaries, such as sea breezes and the topographic steering by mountains. Indeed, for the 1994 Hawaiian cluster the application of the hybrid model did not provide a statistically significant improvement over advection by the climatological, near-surface currents (not shown). The inclusion of the 9 drifters (out of a total of 30) of this cluster, therefore, has simply lowered the IF values of Fig. 5a throughout the entire (α, γ) matrix. Note, however, that adding this cluster has a much more pronounced effect on the maximal IF value (decrease from 1.336 to 1.205) than on the minimal value (decrease from 0.999 to 0.993 only).

The second point is that, overall, in both Figs. 5a and 5b there are no contours with IF < 1.00; that is, (α, γ) pairs yield trajectories that are not worse than pure advection. The minimal IF of all 30 drifters in Fig. 5b is 0.993 and the maximal IF is 1.205, so the 0.05 contour resolution in Fig. 5b cannot capture the 0.007 difference from 1. For the open-ocean clusters shown in Fig. 5a the minimal IF is only 0.001 smaller than 1.00, so the worst hybrid model trajectories are not significantly worse than advection by the currents. In both cases, for α sufficiently larger than 0.0 the trajectories generated by the hybrid model are significantly closer to the observed ones than pure advection.

The robustness of the IF contours in Fig. 5 implies that the model provides reliable results for clusters of drifters, which indicates that at the best-fitting (α, γ) values improvement can be expected in a statistical sense but not necessarily for each and every drifter. In fact, for three of the 1990 drifters the individual IF values at the best (α, γ) values were found to be less than 1.0. A quick identification of these three drifters showed that these are exactly the same three southern drifters that moved nearly purely westward for the whole 10-day period. Since the winds at 2°N (where these three drifters traveled) were blowing nearly parallel to the climatological currents (see Fig. 2a) *and* to the drifter trajectory, the winds could only deflect the numerical trajectories northward (in the Northern Hemisphere), which will displace these trajectories away from the observed ones. Thus, in cases where the hybrid model provides no improvement over pure advection the reason can be traced to a physical disagreement between

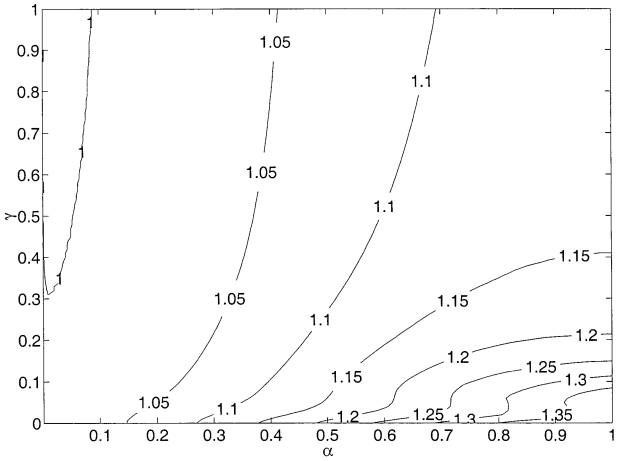

FIG. 6. Contour plot of the average IF(α, γ) over 21 drifter trajectories of the open-ocean 1990 and 1993 clusters using ECMWF wind fields. Maximal IF value is 1.428 and the minimal value is 0.999. The corresponding IF values using NOGAPS winds are shown in Fig. 5a, where the maximal and minimal values are 1.336 and 0.999, respectively.

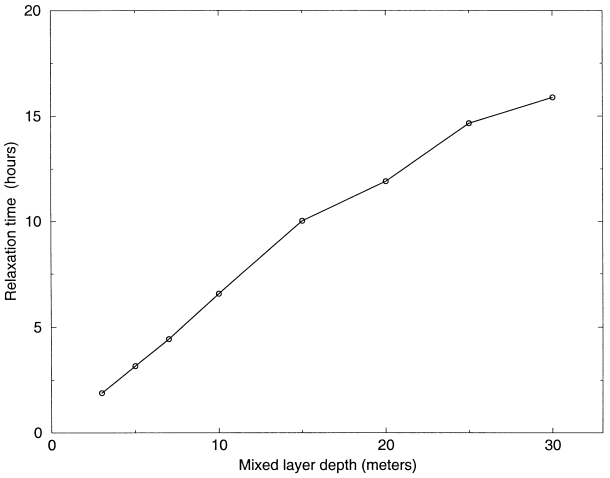

FIG. 7. The change in the value of $1/\gamma^*$ (h) that yields the best IF for $\alpha = 1$ as a function of Ekman depth H (m) [recall that δ in Eqs. (2.3a) and (2.3b) equals H/R]. Wind forcing is provided by NOGAPS and the observed trajectories belong to the 21 drifters of the open-ocean 1990 and 1993 clusters.

the steady, wind-driven, Ekman trajectories and the observed trajectories.

The best predicted trajectories for drifter ID number 11668, 11676, and 11706, from the 1990 cluster had α values of 0.0. These drifters, the southernmost drifters in Fig. 2a, are in the South Equatorial Current (SEC), which is well represented in the climatological mean flow. We presume that in well-defined strong current regimes, like equatorial jets and western boundary currents, the hybrid model offers little improvement over advection by well-documented climatological currents. The low latitude of these trajectories (2°N) might be the reason that Ekman dynamics does not dominate their motion.

c. The effect of wind fields' temporal resolution

The IF contours of the 21 open-ocean trajectories (1990, 1993 clusters) forced by NOGAPS winds (Fig. 5a) can be compared to the IF contours calculated with ECMWF winds that have 4-times-higher temporal resolution (Fig. 6). Here, the maximal average IF is higher than with NOGAPS winds (1.428 versus 1.336) but the minimal IF is 0.999, exactly the same as with NOGAPS winds (i.e., minimal IF is insignificantly smaller than 1.00 in both wind fields). Since the spatial resolutions of the two fields are only slightly different (1.125° versus 1.25°) the main improvement attained with ECMWF fields seems to result from their 4-times-higher temporal resolution. The best value of α equals 1.0 for both fields but the best γ value in ECMWF fields is somewhat lower, implying a longer relaxation time. In order to ascertain that the improvement attained with the ECMWF winds is indeed due to their higher resolution we generated IF contours for trajectories calculated with daily averages of the same ECMWF fields. This calculation resulted in maximal IF of 1.275 (obtained with $\alpha = 1$; $\gamma = 0.02$), which is smaller than both IF = 1.428 obtained with 4 per day ECMWF fields and IF = 1.336 obtained with 1 per day NOGAPS winds. Thus, forcing the model with higher-resolution winds leads to more accurate drifter trajectories.

d. The effect of Ekman depth

All drifters in the present study were drogued at 15 m, while the results shown in the preceding sections were computed for an Ekman depth of 30 m, which was shown in Lagerloef et al. (1999) to be the relevant depth in the tropical Pacific Ocean. Since predictive power is also required in search and rescue operations, where the objects extend only a few meters below the ocean's surface, a comparison with results calculated for a thinner Ekman depth is in order.

It is clear that when the Ekman depth is thin, the same wind stress will constitute a stronger forcing in our vertically averaged model, which will yield an increased acceleration. Thus, in order for the correctional velocity not to become too large the friction coefficient, γ, should be increased. This issue is accentuated by the fact that the best IF values occur near $\alpha = 1$, so the correctional velocity provides nearly all the advection velocity of the drifter. Indeed, these findings are confirmed by the results shown in Fig. 7, in which the values of $1/\gamma^*$ that yield the best IF values for $\alpha = 1.0$ increase monotonically with the Ekman depth $-$ H [note: δ in Eqs. (2.3a,b) equals H/R]. It is also apparent from these results that the increase of $1/\gamma^*$ with H is nearly linear, though the reason for it is not quite clear. As before, trajectory length is 10 days, and a look at other trajectory lengths is now in order.

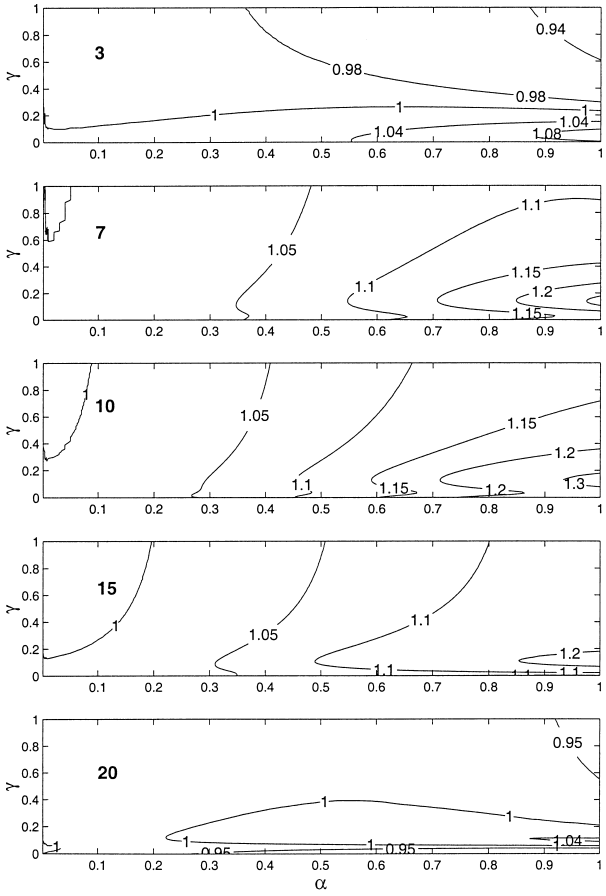

FIG. 8. The IF contours are, from top to bottom, 3-, 7-, 10-, 14-, and 20-day-long trajectories using NOGAPS winds for the open-ocean clusters. For short and long trajectories most IF values are smaller than 1.00, indicating that at long times, the errors in the wind dominate the trajectory.

e. Trajectory length

All calculations up to this point were made for 10-day-long trajectories. For long trajectories one can expect the wind correction to the climatological currents to diminish, since by definition the climatological currents become more meaningful at long time scales. However, this expectation may be false due to the chaotic nature of Lagrangian drifters and short correlation time scales of near-surface motions. After a few days to a week, drifter velocities along a trajectory are no longer correlated. The chaotic nature of Eqs. (2.2a) and (2.2b) implies a sensitivity of Eqs. (2.3c) and (2.3d) to the exact (α, γ) values. Optimal α values for individual trajectories were usually near 0.0 or 1.0, indicating a non-Gaussian, bimodal α distribution such as that found in strongly nonlinear systems.

For much shorter trajectories the temporal resolution of the winds (1 per day for NOGAPS fields) and the use of zero initial velocity imply that order 1-day-long trajectories are not expected to be accurately calculated by our model. The general features of all IF contours

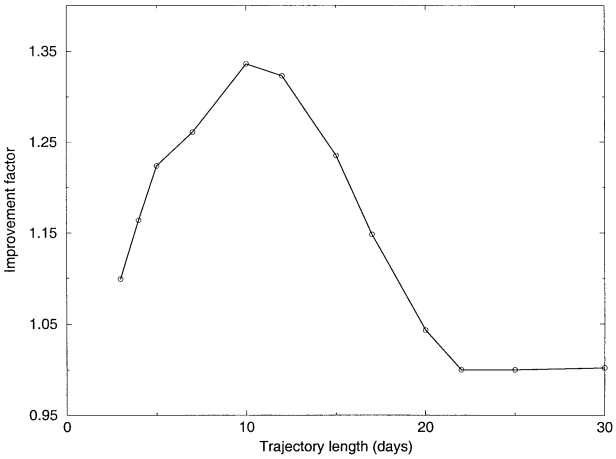

FIG. 9. The variation of maximal IF value with the trajectory length. Wind forcing is by NOGAPS fields. For all trajectory lengths between 3 and 20 days the maximum IF occurs at $\alpha = 1$.

of 5- to 15-day-long trajectories are very similar to those of the 10-day-long contours shown in Fig. 5a. As is clear from the middle three panels of Fig. 8, there are no contours with IF < 1.0, and the maximal IF value obtains for $\alpha = 1.00$ and γ of order 0.15. However, for 3- and 20-day-long trajectories the IF contours in Fig. 8 have a significantly different pattern: most (α, γ) pairs yield IF < 1.00 and [1.0 $-$ minimum(IF)] $>$ [maximum(IF) $-$ 1.0], implying that the worst-case trajectories outweigh the best-case ones.

The variation of the maximal IF value with trajectory length is shown in Fig. 9. The maximal IF value occurs for 10-day-long trajectories. Above 3 weeks and below 3 days, the hybrid model does not afford a significant improvement. The climatological currents are based on a spline fit to all data in each given month, so it best captures monthly time scales. Because of the chaotic nature of oceanic trajectories and the inaccuracies in the wind, the prediction errors for the wind-driven particle model grow rapidly with time. At short time scales of 3 days, on the other hand, the use of zero initial velocity seems to be the culprit for the poor performance of the hybrid model (see section 4f). High-resolution ECMWF winds improve the Lagrangian prediction on short time scales: maximal IF for 3-day trajectories is 1.2 versus 1.1 with NOGAPS (in both cases, best IF values are obtained with $\alpha = 1$). However, for 1-day-long trajectories even ECMWF winds yield maximal IF of 1.009, that is, no significant improvement over pure advection.

f. Initial velocity

The effect of initializing the hybrid model with $\mathbf{V}_{\rm cor}(t = 0) = [\mathbf{V}_{\rm obs} - (1 - \alpha)\mathbf{V}_{\rm clim}]/\alpha$ (where $\mathbf{V}_{\rm obs}$ is the observed drifter velocity at $t = 0$) instead of $\mathbf{V}_{\rm cor}(t = 0) = 0$ is studied here for 3-day-long trajectories using ECMWF [a similar effect of $\mathbf{V}_{\rm cor}(t = 0) \neq 0$ occurred with NOGAPS winds]. The results shown in Fig. 10 for

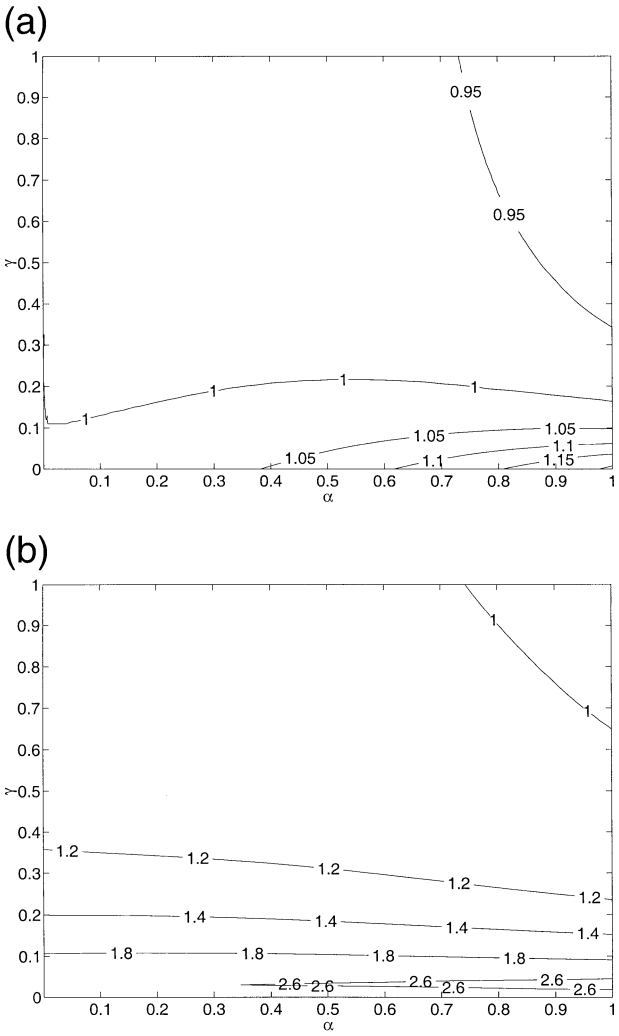

FIG. 10. The IF contours for 3-day-long trajectories when the hybrid model is forced by ECMWF winds and initialized with (a) $\mathbf{V}_{cor}(t = 0) = 0$ and (b) $\mathbf{V}_{cor}(t = 0) = (\mathbf{V}_{obs} - (1 - \alpha)\mathbf{V}_{clim})/\alpha$ [where $\mathbf{V}_{obs}$ is the observed drifter velocity, i.e., $\mathbf{V}_{dr}(t = 0) = \mathbf{V}_{obs}(t = 0)$]. The best IF value of the hybrid model initialized by the observed drifter velocity is 2.79, compared with the persistence model—$\mathbf{V}_{dr}(t) = \mathbf{V}_{obs}(t = 0)$—of 1.5 only

ECMWF winds convincingly demonstrate that the use of the correct initial velocities greatly improves the performance of the hybrid model. The maximum IF value of 1.208 in Fig. 9a increases to 2.790 in Fig. 10b due only to the incorporation of the observed initial velocity in the calculations (both maximal IF values occur at $\alpha = 1.0$ and low $\gamma < 0.03$), and the corresponding minimal IF values increase slightly (from 0.917 to 0.963). Also, for γ values between about 0.15 and 0.65 all IF values that are smaller than 1.0 when the model is initialized with zero velocity become larger than 1.0 when the observed velocity is used in the model's initialization. A comparison of Fig. 10a with Fig. 8a further demonstrates the effect that an increase in temporal resolution of the wind fields has on the performance of the

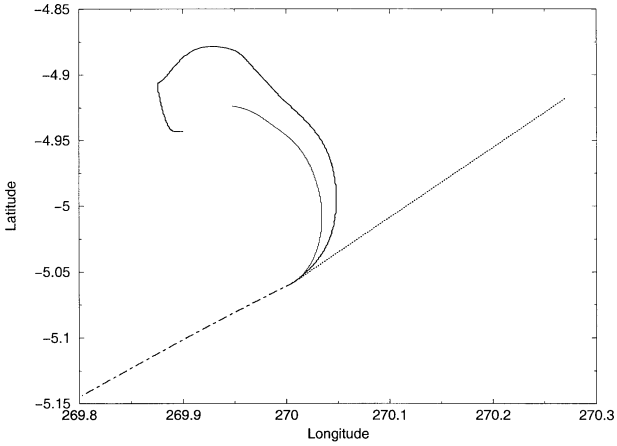

FIG. 11. A comparison between the 3-day-long trajectories generated by observation of drifter no. 25 of the 1993 cluster (thick solid line), advection by the climatological currents (dot–dashed line), persistence—i.e., advection by the observed initial velocity (dotted line), and the best ($\alpha = 1$, $\gamma = 0.08$) trajectory of the hybrid model forced by ECMWF winds (thin solid line) and initialized with the observed initial velocities. The two former models completely miss the observed inertial loop caused by the wind forcing while the hybrid model captures many of its overall features. Note also that the observed initial drifter velocity (indicated by the persistence line) is directed opposite to the climatological currents.

hybrid model. When the model is forced by ECMWF winds (Fig. 10a) that have four fields per day the maximal IF increases to 1.208 from the 1.099 value it has when the model is forced by NOGAPS winds (Fig. 8a) that only have one field per day. The corresponding minimal IF values are hardly changed.

The improvement of the hybrid model for all 21 trajectories can be compared to a simple model—persistence—where one assumes that the drifter velocity remains unchanged with time, that is, $\mathbf{V}_{dr}(t) = \mathbf{V}_{obs}(t = 0)$. The IF value afforded by the persistence model for the drifters shown in Fig. 10 is only 1.5 compared with 2.79 best IF value of the hybrid model.

An inspection of the four trajectories of drifter number 25 (observed, hybrid model, climatological, and persistence) shows (Fig. 11) that the observed inertial loop caused by the wind forcing is partially captured by the hybrid model but it is totally missed by the other two. It also demonstrates that the persistence trajectory is directed 180° to the climatological currents!

5. Discussion and concluding remarks

The simple and practical model presented in this study employs the best available estimates of the wind stress to calculate a correction to the climatological surface currents. This approach differs fundamentally from traditional methods in which this correction is assumed to have a known form (e.g., Gaussian with zero mean), and only the parameters of this form are updated at each time step based on previous times' calculations (e.g., Özgökmen et al. 2000, 2001). The application of wind

data, and not a different algorithm for updating/calculating a parameter such as the variance of the current, is the novelty of the present approach. It also differs from dynamical models of wind-driven particle trajectories (e.g., Paldor 2002), in which the nonlinear terms result in chaotic trajectories.

Comparing our model with that of Lagerloef et al. (1999) one can interpret our $\mathbf{V}_{cor}$ as the time-dependent counterpart of their $\overline{\mathbf{U}}_e$—the average velocity of the Ekman layer. In order to make the correspondence, one has to substitute $\mathbf{V}_{clim}$ of Eq. (2.1) for the pressure gradient term in Lagerloef et al.'s Eqs. (1) and (2) using the geostrophic relationship. Their total velocity, $\mathbf{V}$, is simply the sum of $\overline{\mathbf{U}}_e$ and this geostrophic velocity, all of which are steady. Since our model is time dependent, it is not surprising that it has a time-dependent correction velocity that satisfies the differential equation, with time-dependent coefficients (2.3a) and (2.3b). Our linear combination coefficients, α, and $(1 - \alpha)$ are the counterparts of the two ''empirical regression coefficients,'' a_1 and a_2 (which do not necessarily add up to 1), that define the drifter velocity in Lagerloef et al.'s Eq. (9).

The negligible contribution of $\mathbf{V}_{clim}$, as well as the dominance of the wind-driven motion, in our study is in contrast to the results reported in Ralph and Niiler (1999). We speculate that in regions like the Gulf Stream, the use of feature or contour-based methods (Mariano and Chin 1996), and the use of satellite data for detecting the near-real-time position of the current will lead to better estimates of $\mathbf{U}$ [in Eq. (1.1), i.e., $\mathbf{V}_{clim}$] and hence to more accurate trajectory predictions. Future use of satellite data for incorporating eddy/vortex structures that are not well represented in $\mathbf{V}_{clim}$ [see the discussion in Kennan and Flament (2000) regarding the contribution of an instability vortex to drifter trajectories in the Tropics] will greatly improve the reconstruction of drifter trajectories in strong eddy fields by the hybrid model developed in this work.

The main findings of this study can be summarized as follows.

The wind stress provides the main forcing for drogued drifter trajectories at the ocean's surface on time scales shorter than 20 days. Therefore, reliable, real-time wind fields are required for an accurate prediction/reconstruction of these trajectories. The role of climatological, near-surface currents is negligible for these trajectories unless the region is well sampled and a strong current dominates the surface dynamics. This conclusion agrees with the result obtained by Özgökmen et al. (2001), who found that advection by the climatological flow field is not a good indicator of drifter motion, but it does not hold in well-sampled, strong-current regimes and it contradicts the results of Ralph and Niiler (1999).

The relaxation time (i.e., the *e*-folding decay time of the drifters' velocity) for 5- to 15-day-long trajectories varies between 0.5 and 1 day, but the best α value is 1.0 for all trajectories shorter than 20 days. For trajectories longer than 20 days the wind-field errors dominate the corrections to the climatological currents.

Higher resolution of the wind fields results in significantly more accurate trajectories.

The model's typical improvement over advection by the climatological currents is 20%–35% in the open ocean depending on the wind field and with zero initial velocity. In the presence of coasts the improvement of the model is greatly reduced since the boundary condition of no-normal flow is not imposed in the model and since the coarse-resolution wind products used in this study do not adequately represent the smaller-scale wind fields near the coast. For nearly all (α, γ) pairs the hybrid model generates more accurate trajectories than advection by the climatological currents.

Accurate initial velocities are crucial for an accurate simulation of trajectories shorter than 3 days, but their effect diminishes with the trajectory's length. When an accurate initial velocity exists the hybrid model performs significantly better than persistence (IF of 2.8 versus 1.5).

For an Ekman depth thinner than 30 m one only has to increase the drag coefficient, that is, shorten the relaxation time, to obtain significant improvements.

Acknowledgments. Financial support for this work was provided by the U.S. Office of Naval Research via Research Grants N00014-99-1-0049 and N00014-95-1-0257 awarded to RSMAS/UM and by the U.S.–Israel Bi-National Science Foundation via a grant to the Hebrew University of Jerusalem.

REFERENCES

Aref, H., 1984: Stirring by chaotic advection. *J. Fluid Mech.,* **243,** 1–21.

——, 1990. Chaotic advection of fluid particles. *Philos. Trans. Roy. Soc. London A,* **333,** 273–288.

Bauer, S., M. S. Swenson, A. Griffa, A. J. Mariano, and K. Owens, 1998: Eddy-mean flow decomposition and eddy-diffusivity estimates in the tropical Pacific Ocean. I. Methodology. *J. Geophys. Res.,* **103** (C13), 30 855–30 871.

——, ——, and ——, 2002: Eddy mean flow decomposition and eddy diffusivity estimates in the tropical Pacific Ocean: 2. Results. *J. Geophys. Res.,* **107,** 3154, doi:10.1029/2000JC000613.

Berloff, P. S., and J. C. McWilliams, 2002: Material transport in oceanic gyres. Part II: Hierarchy of stochastic models. *J. Phys. Oceanogr.,* **32,** 797–830.

Bower, A. S., 1991: A simple kinematic mechanism for mixing fluid parcels across a meandering jet. *J. Phys. Oceanogr.,* **21,** 173–180.

Castellari, S., A. Griffa, T. M. Özgökmen, and P.-M. Poulain, 2001: Prediction of particle trajectories in the Adriatic Sea using Lagrangian data assimilation. *J. Mar. Syst.,* **29,** 33–50.

Davis, R. E., 1982: On relating Eulerian and Lagrangian velocity statistics: Single particles in homogeneous flows. *J. Fluid Mech.,* **114,** 1–26.

Dutkiewics, S., and N. Paldor, 1994: On the mixing enhancement in a meandering jet due to the interaction with an eddy. *J. Phys. Oceanogr.,* **24,** 2418–2423.

Dvorkin, Y., N. Paldor, and C. Basdevant, 2001: Reconstructing balloon trajectories in the tropical stratosphere with a hybrid model

using analysed fields. *Quart. J. Roy. Meteor. Soc.,* **127** (573A), 975–988.

Flierl, G. R., 1981: Particle motions in large amplitude wave fields. *Geophys. Astrophys. Fluid Dyn.,* **18,** 39–74.

Garfield, N., M. E. Maltrud, C. A. Collins, T. A. Rago, and R. G. Paquette, 2001: Lagrangian flow in the California Undercurrent, an observation and model comparison. *J. Mar. Syst.,* **29,** 201–220.

Garraffo, Z. D., A. J. Mariano, A. Griffa, C. Veneziani, and E. P. Chassignet, 2001a: Lagrangian data in a high-resolution numerical simulation of the North Atlantic I. Comparison with in situ drifter data. *J. Mar. Syst.,* **29,** 157–176.

——, A. Griffa, A. J. Mariano, and E. P. Chassignet, 2001b: Lagrangian data in a high-resolution numerical simulation of the North Atlantic II. On the pseudo-Eulerian averaging of Lagrangian data. *J. Mar. Syst.,* **29,** 177–200.

Gill, A. E., 1982: *Atmosphere–Ocean Dynamics.* Academic Press, 662 pp.

Griffa, A., 1996: Applications of stochastic particle models to oceanographic problems. *Stochastic Modelling in Physical Oceanography,* R. J. Adler, P. Muller, and B. L. Rozovskii, Eds., Birkhauser, 114–140.

Hansen, D. V., and P-M. Poulain, 1996: Quality control and interpolations of WOCE–TOGA drifter data. *J. Atmos. Oceanic Technol.,* **13,** 900–909.

Käse, R. H., and D. J. Olbers, 1979: Wind-driven inertial waves observed during phase III of GATE. *Deep-Sea Res.,* **26** (Suppl. 1), 191–216.

Kennan, S. C., and P. J. Flament, 2000: Observations of a tropical instability vortex. *J. Phys. Oceanogr.,* **30,** 2277–2301.

Kundu, P. K., 1976: An analysis of inertial oscillations observed near the Oregon coast. *J. Phys. Oceanogr.,* **6,** 879–893.

Lagerloef, G. S. E., G. T. Mitchum, R. B. Lukas, and P. P. Niller, 1999: Tropical Pacific near-surface currents estimated from altimeter, wind and drifter data. *J. Geophys. Res.,* **104** (C10), 23 313–23 326.

Mariano, A. J., and T. M. Chin, 1996: Feature and contour-based data analysis and assimilation in physical oceanography. *Stochastic Modelling in Physical Oceanography,* R. J. Adler, P. Muller, and B. L. Rozovskii, Eds., Birkhauser, 311–342.

——, E. H. Ryan, B. D. Perkins, and S. Smithers, 1995: The Mariano Global Surface Velocity Analysis 1.0. U.S. Coast Guard Rep. CG-D-34-95, 55 pp.

McClean, J. L., P.-M. Poulain, J. W. Pelton, and W. E. Maltrud, 2002: Eulerian and Lagrangian statistics from surface drifters and a high-resolution POP simulation in the North Atlantic. *J. Phys. Oceanogr.,* **32,** 2472–2491.

Niiler, P. P., 2001: The World Ocean Surface Circulation. *Ocean Circulation and Climate-Observing and Modelling the Global Ocean,* G. Siedler, J. Church, and J. Gould, Eds., Academic Press, 193–204.

Özgökmen, T. M., A. Griffa, A. J. Mariano, and L. I. Piterbarg, 2000: On the predictability of Lagrangian trajectories in the ocean. *J. Atmos. Oceanic Technol.,* **17,** 366–383.

——, L. I. Piterbarg, A. J. Mariano, and E. Ryan, 2001: Predictability of drifter trajectories in the tropical Pacific Ocean. *J. Phys. Oceanogr.,* **31,** 2691–2720.

Paduan, J. D., and P. P. Niiler, 1993: Structure of velocity and temperature in the North-East Pacific as measured with Lagrangian drifters. *J. Phys. Oceanogr.,* **23,** 585–600.

Paldor, N., 2002: The transport in the Ekman surface layer on the spherical Earth. *J. Mar. Res.,* **60,** 47–72.

——, and P. D. Killworth, 1988: Inertial trajectories on the rotating Earth. *J. Atmos. Sci.,* **45,** 4013–4019.

——, Y. Dvorkin, and C. Basdevant, 2001: Improving the calculation of particle trajectories in the extratropical troposphere using standard NCEP fields. *Atmos. Environ.,* **36,** 483–490.

Pasquero, C., A. Provenzale, and A. Babiano, 2001: Parameterization of dispersion in two-dimensional turbulence. *J. Fluid Mech.,* **439,** 279–303.

Pollard, R. T., and R. C. Millard, 1970: Comparison between observed and simulated wind-generated inertial oscillations. *Deep-Sea Res.,* **17,** 813–821.

Ralph, E. A., and P. P. Niiler, 1999: Wind-driven currents in the tropical Pacific. *J. Phys. Oceanogr.,* **29,** 2121–2129.

Rao, R. R., R. L. Molinari, and J. F. Festsa, 1989: Evolution of the climatological near-surface thermal structure of the tropical Indian Ocean. Part I: Description of mean monthly mixed layer depth and sea-surface temperature, surface current, and surface meteorological fields. *J. Geophys. Res.,* **94** (C8), 10 801–10 815.

Thomson, D. J., 1986: A random walk model of dispersion in turbulent flows and its application to dispersion in a valley. *Quart. J. Roy. Meteor. Soc.,* **112,** 511–529.

——, 1987: Criteria for the selection of stochastic models of particle trajectories in turbulent flows. *J. Fluid Mech.,* **180,** 529–556.